Using Alternatives to Determine the Shallowest Depth for Bathymetric Charting

Case Study

Mohammadloo, Tannaz H.; Snellen, Mirjam; Simons, Dick G.; Dierikx, Ben; Bicknese, Simon

Important note
To cite this publication, please use the final published version (if applicable).
Please check the document version above.

Case Study

Using Alternatives to Determine the Shallowest Depth for Bathymetric Charting: Case Study

Tannaz H. Mohammadloo[1]; Mirjam Snellen, Ph.D.[2]; Dick G. Simons, Ph.D.[3]; Ben Dierikx, M.Sc.[4]; and Simon Bicknese[5]

Abstract: Methods for gridding multibeam echo sounder (MBES) measurements to equidistant grids are proposed as alternatives to the shallowest measured depth, which is affected by outliers. The approaches considered use a combination of mean and standard deviation of soundings and the regression coefficient from the best fitted plane. These methods along with mean and shallowest depths were applied to two surveyed areas. Two issues were found to be of importance, that is, a proper distribution of soundings and low uncertainties in the depth measurements. Improper sampling excludes using the method employing regression coefficients. For flat areas, the shallowest measured depth was found to be highly influenced by measurement uncertainties, counteracted when using the mean depth. However, the mean depth underestimates the shallowest depth for areas with slopes. When correcting the mean depth for standard deviation, the effect of slopes is accounted for while the influence of measurement uncertainties is decreased compared to shallowest measured depth. Since the uncertainties are dependent on beam angle, depth, and measurement equipment, these issues need to be accounted for in survey planning. **DOI: 10.1061/(ASCE)SU.1943-5428.0000278.** © *2019 American Society of Civil Engineers.*

Author keywords: Bathymetry gridding; Standard deviation of depth measurements; Regression coefficients; Mean depth; Shallowest depth.

Introduction

Reliable information about sea- and riverbed bathymetry is of great interest for a large number of applications, such as maintaining safe navigation, building off-shore constructions, and making nautical charts. Nowadays, multibeam echo sounders (MBESs) provide high spatial coverage at relatively limited costs, and hence have been extensively used for bathymetric measurements. The amount of data generated by an MBES depends on the ping rate and the number of beams in the across-track direction. As an example, for a Kongsberg EM 3002 MBES (Kongsberg, Norway), the maximum ping rate is 40 Hz and the number of beams in the single-head mode is 254, which results in an incoming data flow of approximately 36.5 million data points per hour (Kannan et al. 2015). Therefore, reduction of the data is necessary for computationally effective processing.

A number of scholars studied approaches for producing a bathymetry map from the soundings collected in an MBES survey, which will be discussed in the subsequent paragraphs. This paper presents and compares a number of methods for producing such maps (without the need for a priori knowledge of the measurement uncertainties) and investigates their feasibility.

Triangulation or equidistant grids are often used for data reduction (Brouns et al. 2001, 2003). Triangular-based gridding is appropriate when measurements are at discrete points. It is flexible with respect to the different levels of detail, that is, a denser triangle pattern is an indication of more detailed relief information. However, this method has large memory requirements and long processing time, and requires sophisticated geometric computations (De Wulf et al. 2012b). The advantages of equidistant grids are their simplicity and low memory requirements. The use of equidistant points enables storing only the depth values (De Wulf et al. 2012a). Since the surveyed areas used in this study were homogeneously surveyed, only equidistant grids were considered.

A commonly used method for assigning depths to the grid of high-density bathymetry data is to use the shallowest (minimum) measured depth within a cell (De Wulf et al. 2012b). The advantage of this approach is that the method preserves the shallowest depth, which is of high importance for safe navigation. The disadvantage, however, is that these shallowest depths can correspond to outliers, and consequently the resulting charted soundings can be (significantly) shallower than the true depth in the area. It is sometimes seen that measurements from the less reliable outer beams, subjected to the largest uncertainties, are selected as the depths to be charted. They are thus more frequently shallower than other measurements in the area (Calder and Mayer 2003). In order to mitigate the effect of measurement errors on the charted depths, it is possible to use other statistics derived from the data. A straightforward approach is to use the mean value (De Wulf et al. 2012b). However, a problem associated with assigning the mean depth is that hazardous objects might be left undetected, and hence safe navigation is

[1]Ph.D. Candidate, Acoustics Group, Dept. of Control and Operations, Faculty of Aerospace Engineering, Delft Univ. of Technology, Kluyverweg 1, 2629 HS, Delft, Netherlands (corresponding author). ORCID: https://orcid.org/0000-0003-0340-1718. Email: T.Hajimohammadloo@tudelft.nl

[2]Associate Professor, Acoustics Group, Dept. of Control and Operations, Faculty of Aerospace Engineering, Delft Univ. of Technology, Kluyverweg 1, 2629 HS, Delft, Netherlands.

[3]Professor, Acoustics Group, Dept. of Control and Operations, Faculty of Aerospace Engineering, Delft Univ. of Technology, Kluyverweg 1, 2629 HS, Delft, Netherlands.

[4]Technical Manager, Rijkswaterstaat Centrale Informatievoorziening en GegevensAnalyse, Derde Werelddreef 1, 2622 HA, Delft, the Netherlands.

[5]Technical Advisor, Rijkswaterstaat Centrale Informatievoorziening en GegevensAnalyse, Derde Werelddreef 1, 2622 HA, Delft, the Netherlands.

prohibited (Mohammadloo et al. 2018). A more advanced approach for assigning a depth to a set of predefined nodes is to use the Combined Uncertainty and Bathymetry Estimator (CUBE) algorithm developed by Calder and Mayer (2001, 2003). This approach constructs a grid over a surveyed area and assigns to each grid node an estimate of depth and its uncertainty. Use is made of a priori standard deviation for the soundings based on the uncertainty model of Hare (1995). At a node, soundings are integrated to obtain an estimate of the depth and uncertainty using an optimal Kalman filter. In the present paper, the main focus is on more straightforward approaches that do not need a priori estimates of the standard deviation of the soundings and use the statistics derived from the measurements. However, the comparison between the approaches presented and CUBE was made to assess their agreement and possible discrepancies. Moreover, the bathymetric uncertainties derived from the measurements were compared to those modeled using Hare (1995), which is also used in CUBE to define a priori estimate of the sounding uncertainties. This provides one with insight into how realistic the modeling is, and it can also give direction for future improvements of the modeling.

The surveyed areas considered in this contribution are located in the Netherlands. The Netherlands is the home of international river basins, such as Scheldt and Ems, which run through the country toward the North Sea and the Wadden Sea. These rivers and the estuaries connecting them to the sea are used for inland waterway transport within the Netherlands and also between the Netherlands and neighboring countries. A shallowest depth has to be guaranteed to keep the rivers navigable and also to ensure that the ships can carry maximum cargo. Currently, for the production of the charts, the Dutch Ministry of Infrastructure and Water Management [Rijkswaterstaat (RWS)] uses the shallowest depth at its measured position from the point cloud of the MBES measurements. The resulting unequal spacing between the points results in high memory requirements. In addition, assigning the shallowest depth can result in an artificially shallow grid as described previously. In this study, the use of alternative techniques for mitigating these two drawbacks was investigated. While the first issue can be easily solved by considering the cell center instead of the location of the shallowest depth, the second issue requires more careful consideration. This second issue, that is, to assign to each cell a depth value that optimally represents the actual shallowest depth, was investigated by considering a number of methods for shallowest depth determination and applying them to two different surveyed areas located in the Westerschelde estuary connecting the Scheldt River to the North Sea, an important shipping route to the port of Antwerp, Belgium. The resulting grids were compared to their shallowest and mean counterparts. This work is part of an effort to investigate future data management for bathymetric measurements in the Netherlands.

Description of Methods for Determining the Shallowest Depth

In general, when using an MBES system, the density of the measurements acquired is high. Table 1 gives the data sets considered in this paper. Consequently, several soundings will be located within a single cell, provided that a large enough cell size is considered. Here, a cell size G was considered in both easting and northing directions, that is, the resolution of the grid in both directions was equal. The number of soundings in each cell is indicated by N_{hits}. The shallowest measured depth corresponds to the measurement out of the N_{hits} soundings that provides the shallowest depth.

Table 1. Covered area, number of soundings, number of cells, and the MBES employed for areas A and B

Parameter	Surveyed area	
	A	B
Area (m²)	4,758,203	4,492,155
Soundings	58,777,805	114,934,172
Cells	4,758,203	4,492,155
MBES	Norbit WBMS	Kongsberg EM 3002D

Note: WBMS = wideband multibeam sonar (Norbit, Trondheim, Norway).

Shallowest Depth Based on the Mean and Standard Deviation

As mentioned, the problem associated with the shallowest depth is that it is not necessarily a good observable because no averaging is carried out to mitigate the effect of measurement errors. However, using the mean depth, $\overline{d}$, neglects the presence of slopes. Therefore, $d_{\min_{c\sigma}}$ is proposed where the standard deviation is subtracted from the mean to account for the measured depth variations within a cell as

$$d_{\min_{c\sigma}} = \overline{d} - c\sigma \tag{1}$$

where c = number of times the standard deviation is subtracted. For example, $d_{\min_{1\sigma}}$ denotes the shallowest depth in the $1 - \sigma$ confidence level (68.3% confidence interval), where σ is the standard deviation of the raw soundings within a cell. Within this research, only $c = 0$ and $c = 1$ (where $c = 0$ indicates that the mean depth is used) were considered.

Shallowest Depth Based on the Regression Coefficients

As a second approach, where the potential presence of slopes along the cell surface is explicitly accounted for, a linear plane is fitted through the depth measurements as

$$f = C_X X + C_Y Y + b - d = 0 \tag{2}$$

where X, Y, and d = easting, northing, and depth of a sounding in a cell, respectively; C_X and C_Y = regression coefficients, representing slopes in easting and northing directions, respectively; and b = constant parameter.

Now we define $\boldsymbol{d} = [d_1, d_2, \ldots, d_{N_{hits}}]^T$ as the vector containing the depth measurements in a cell. Vector $\hat{\boldsymbol{a}} = [b, C_X, C_Y]^T$ contains the unknown parameters. The model for the observations can be written as

$$E\{\boldsymbol{d}\} = A\hat{\boldsymbol{a}} \tag{3}$$

where E is the expectation operator; and A is the design matrix of size $N_{hits} \times 3$, of which the ith row is $A_i = [1, X_i, Y_i]$. The unknown parameters can be derived by minimizing the quadratic error ($\| e \|^2$, where $\| \cdot \|$ denotes the norm of a vector) between the linear regression and the real depth measurements [i.e., $\| e \|^2 = (\boldsymbol{d} - A\hat{\boldsymbol{a}})^T (\boldsymbol{d} - A\hat{\boldsymbol{a}})$]. The estimate of the vector $\hat{\boldsymbol{a}}$, assuming independent identically distributed measurements, is (Teunissen et al. 2006)

$$\hat{\boldsymbol{a}} = (A^T A)^{-1} A^T \boldsymbol{d} \tag{4}$$

Substituting easting and northing of the measurements in the matrix A leads to rank deficiency of the normal matrix ($N = A^T A$), also referred to as numerical instability, due to the difference in the

magnitude of the columns of the design matrix. To solve this problem, the equation of the plane can be alternatively defined as

$$f = C_X(X - \overline{X}) + C_Y(Y - \overline{Y}) - d + \underbrace{(b + C_X\overline{X} + C_Y\overline{Y})}_{b'} = 0 \quad (5)$$

where $\overline{X}$ and $\overline{Y}$ = mean (expected) values of the easting and northing in a cell, respectively. Thus, the unknown parameters are now of the form $\hat{a} = [b', C_X, C_Y]^T$.

Using Eq. (4) with $A_i = [1, X_i - \overline{X}, Y_i - \overline{Y}]$ as the design matrix, one can determine the unknown parameters. The least-squares estimator of observables ($\hat{d}$) and of residuals ($\hat{e}$) follows from

$$\hat{d} = A\hat{a}$$

$$\hat{e} = d - A\hat{a} \quad (6)$$

where $\hat{d}$ and $\hat{e}$ represent the depth measurements projected onto the range space of matrix A (the plane) and the deviation of the bottom topography from the best-fitted plane, respectively. The depth residuals are normally distributed with zero mean and standard deviation σ_{corr}. This standard deviation along with the least-squares estimator of the observable is used to construct a confidence limit for the identification and rejection of the outliers (Artilheiro 1998).

The depths at the four corners of a cell are derived using C_X and C_Y and the intercept, determined from substituting Eq. (4) in Eq. (2). The easting and northing of these corners are

$$X_{\text{LU}} = X_{\text{LL}} = X_c - \frac{G}{2}$$

$$Y_{\text{RL}} = Y_{\text{LL}} = Y_c - \frac{G}{2}$$

$$X_{\text{RU}} = X_{\text{RL}} = X_c + \frac{G}{2}$$

$$X_{\text{RL}} = X_{\text{LU}} = Y_c + \frac{G}{2} \quad (7)$$

where the subscripts LU, LL, RL, and RU = upper-left, lower-left, lower-right, and upper-right corners, respectively; and X_c and Y_c = position of the cell center. The shallowest depth based on the regression coefficients ($d_{\text{min}_{\text{Reg}}}$) reads as

$$d_{\text{min}_{\text{Reg}}} = \min(d_{\text{LU}}, d_{\text{LL}}, d_{\text{RL}}, d_{\text{RU}}) \quad (8)$$

where $\min(d_{\text{LU}}, d_{\text{LL}}, d_{\text{RL}}, d_{\text{RU}})$ indicates the shallowest depth among the four depths at the corners of the cell. Theoretically, $d_{\text{min}_{\text{Reg}}}$ is a more realistic representative of the true shallowest depth in a cell compared to the one based on the standard deviation and mean depth because it explicitly takes the effect of potential slopes into account. One can subtract the standard deviation of the depth residuals (which is an indication of the deviation of the bottom topography from the best fitted plane), σ_{corr} from Eq. (8), to ensure a safety margin.

Description of the Data Sets

To assess the effect of using the different methods for shallowest depth determination as introduced in the previous section, two areas in the Westerschelde estuary were considered. The data sets were provided by RWS. These data sets were chosen because they contain regions with significant importance for navigation, related to very shallow depths. Fig. 1 shows the bathymetry of the areas. For the sake of convenience, the areas Honte (omgeving Put van Borssele) and Pas van Terneuzen (Springergeul ankergebied) are referred to as A and B, respectively. The depth varies from 2.5 to 66.20 m in Area A and from 5.10 to 17.70 m in Area B. In Area A, a dredged navigational channel exists (Fig. 1) where the relatively deep area inside the trenches is maintained by constant dredging and maintaining the slopes. Hence, it is interesting to assess the bathymetry in this region using the different approaches for obtaining the shallowest depth. Regarding Area B, it is seen from Fig. 1 that two sets of sand dunes exist, one in the deepest part of the surveyed area and the other in the shallower part. It is important to investigate the impact of using the different measures for shallowest depth on the mapping of sand dunes. Table 1 presents the size of the areas, number of soundings, number of cells, and the MBESs used.

A brief discussion of the systems used for data acquisition and bathymetry processing is needed (vertical positioning in particular). A critical element in the accurate estimation of the depth below the transducer is the sound speed profile (SSP) in the water column, which varies both spatially and temporally. Therefore, sufficient and accurate measurements of this parameter are required. To ensure the former, the surveyors were asked to acquire a new SSP if there was a difference of more than 2 m/s between the surface sound speed value and the surface sound speed from the latest full sound speed profile, as specified by the National Oceanic and Atmospheric Administration (NOAA 2017). The sound velocity profilers employed in Areas A and B were manufactured by Valeport (Totnes, UK) and AML Oceanographic (Sidney, BC, Canada), respectively, and they measure the sound velocity either directly or as a function of conductivity, temperature, and depth. The depth below the transducer was then calculated using ray tracing in the processing software. The accuracy of the sound velocity profiler indicated by the manufacturer is around 0.02 m/s (Valeport 2018; AML Oceanographic 2017). However, from measurements in different locations (inland waterways and the North Sea), the uncertainty was found to be 0.2 m/s, and hence this value was chosen as a more realistic description of the systems' accuracy and was subsequently used to quantify the depth uncertainty induced by the uncertainty in the sound speed profile. A discussion on the effect of using erroneous SSP is provided subsequently.

Both data sets were acquired using QINSy, which was developed by Quality Positioning Service (QPS). Both global navigation satellite system (GNSS) sensors on board received the correction signal from real-time kinematic (RTK) services from the Netherlands Positioning Service (NETPOS). The GNSS antenna position was thus determined with an accuracy of a few centimeters in World Geodetic System 1984 (WGS84). Using RTK for the vertical footprint positioning in QINSy means that the depth relative to the chart or vertical datum was directly measured from accurate GNSS observations. [For more information on different depth processing algorithms available in QINSy, an interested reader may refer to QINSy (2018).] Therefore, the water surface level is of no relevance anymore and accounting for height offsets, such as tide, draft, and height above draft reference, are not necessary for this method, and thus do not affect the quality of the derived depths. Heave measurements (short-term variations in the transducer's depth) are, however, used within the processing software to calculate the height of the vessel's center of gravity between two position updates [because the update rate of the inertial navigation sensor (INS) is higher than that of the GNSS system]. Therefore, the accuracy of heave measurement acquired by the INS contributes to the uncertainty in the estimate of the depth. In addition, potential systematic heave errors result in depth errors through a systematic rise and fall of all the beams (Godin 1998; Hughes Clarke 2003). A careful assessment of the surveyed areas shows that such a systematic behavior does not exist. There are also other contributors affecting
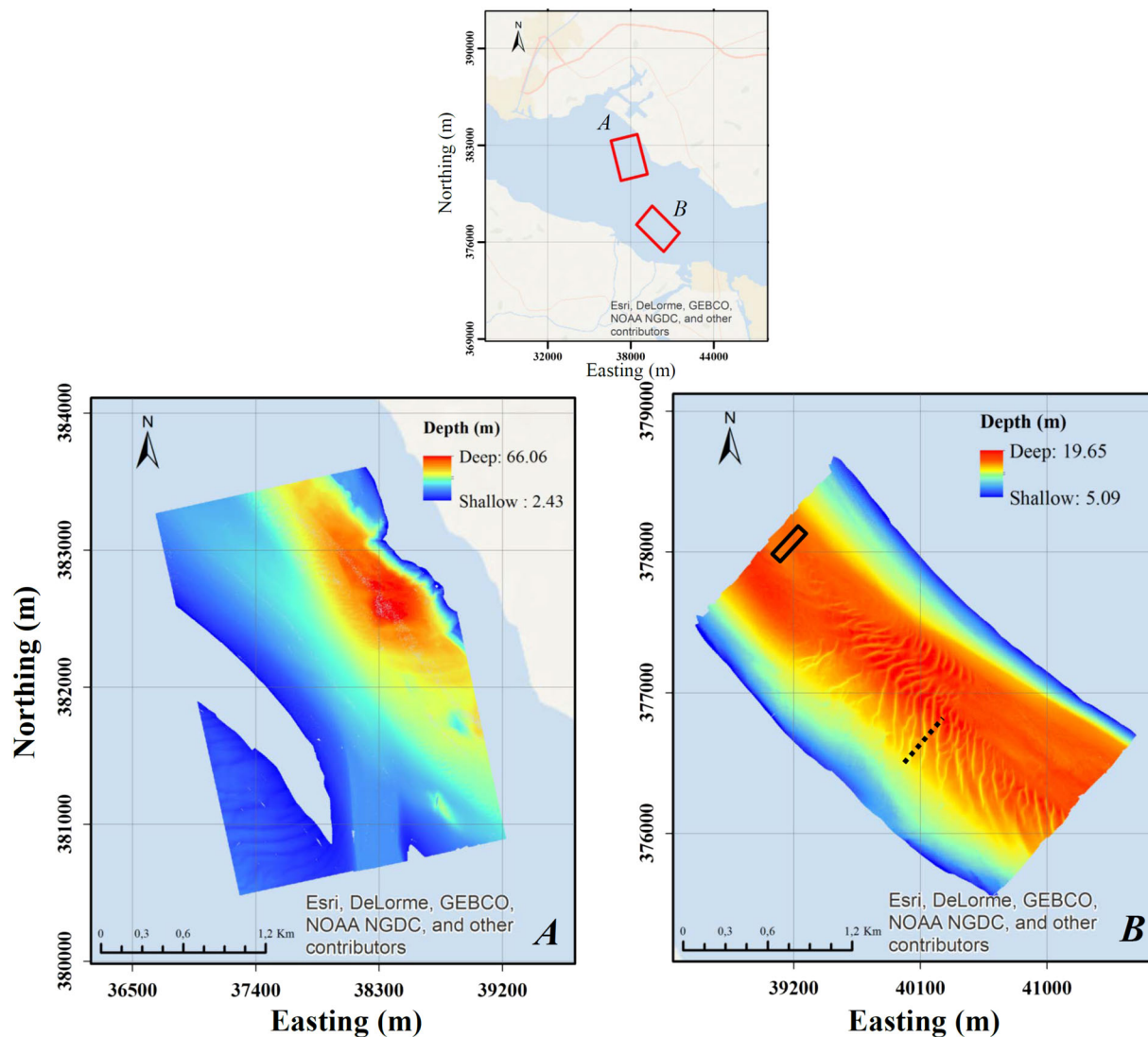
Fig. 1. (Color) Bathymetric maps of the two areas considered: Area A, Honte (omgeving Put van Borssele); and Area B, Pas van Terneuzen (Springergeul ankergebied). The depth is considered positive downward. The black rectangle and black dashed areas in Area B consist of 150 and 30 pings and represent flat and nonflat areas, respectively. (Maps courtesy of Esri, DeLorme, GEBCO, NOAA NGDC, and other contributors.)

the quality of depth measurements that will be discussed in detail in the following.

Results

In this section, the results of determining the shallowest depth in a cell based on the methods described are presented. Before proceeding, a discussion of the cell size is put forward because it affects the grids derived. NOAA (2017) specifies the so-called grid resolution (cell size) as a function of depth. Based on the specification (for full seafloor coverage), for depths ranging from 0 to 20 m, a cell size of 1 m in both directions is required. For depths ranging from 18 to 40 m and from 36 to 80 m, the specified cell sizes are 2 and 4 m, respectively. For Area B, a cell size of 1 m was chosen (see the depth range in Fig. 1). For Area A, based on the specification, the three aforementioned cell sizes can be used depending on the depth. However, the smallest cell sizes have been chosen to minimize the possibility of not mapping the bathymetric features (although this requires higher computing power and larger memory space); a detailed discussion can be found in Maleika (2015).

For the data sets considered here with the specifications presented in Table 2, the across-track distances between the two soundings (in one ping) were around 0.7 and 0.48 m in Areas A and B, respectively; that is, smaller than the cell size. For the along-track resolution of the MBES, the operational ping rate should be considered, which depends on the water depth and the angular sector and can be lower than the theoretical maximum ping rate specified by the manufacturer (Table 2). For the deepest parts of Areas A and B and the outermost beam, the two-way travel times equal 0.192 and 0.073 s, respectively (i.e., ping rates of 5 and 13 Hz). The along-track spacings between the two consecutive pings with the survey speed of nearly 5 m/s are thus equal to 0.96 and 0.36 m, respectively. Based on the preceding discussion, it can be concluded that in general multiple measurements will be within 1×1 m^2, allowing for extraction of the required statistics.

As a first step toward comparing the depths derived from the approaches discussed previously, however, the validity of using the mean was investigated. The shallowest depth using the standard deviation and mean is based on the characteristics of the normal distribution for which it is assumed that an α percentage of depths appear within the range $\overline{d} \pm c\sigma$ (as an example, 68.3% of the data assuming $c = 1$). However, if the distribution of the data is not

normal, the mean and standard deviation cannot automatically be considered as indicators representing the central tendency and variation of the data, respectively. Moreover, the mean and standard deviation are negatively influenced by the outliers (Rousseeuw and Hubert 2011). A measure for the central tendency of the data that can be used instead is the median, with the advantage of being insensitive to the presence of the outliers. In contrast to the mean, which is affected by the presence of even one aberrant value (0% breakdown point), the median can resist up to 50% of outliers (50% breakdown point) (Maronna et al. 2006). As for an indicator of the variability of the data in case of having a skewed (asymmetrical) distribution, one can use the median absolute deviation (MAD), with 50% breakdown point, in contrast to the standard deviation,

with 0% breakdown point. MAD is also a more robust estimate of the data variability than the interquartile range (IQR). The latter is defined as the difference between the third and first quartiles of the data and has 25% breakdown point (Rousseeuw and Hubert 2011), as an example. Considering the higher breakdown point of MAD than IQR, the former was investigated as a potential alternative for the standard deviation.

Fig. 2 shows the depth distribution within four cells with different numbers of soundings. It is seen that for these cells, the distribution of the depth measurements is skewed and it varies from one cell to another due to varying bottom characteristics. Shown in Fig. 3 is the map of the differences between the median and mean depths for Area A. Varying colors are used to represent the differences. Each color represents a certain percentage (25% in this case) of all data points. It is seen that for 50% of the data, the difference between the depth based on the median and mean varies between −0.007 and 0.005 m. For 25% of the cells, the differences vary between 3.254 and −0.007 m; however, for 97% of these cells the differences are less than 0.05 m. The same situation also holds for the upper bounds of the data, that is, for 98% of the cells between the 75th percentile and maximum difference, the differences are less than 0.05 m. The color green in Fig. 3, which is not present in the color bar, is due to the fact that in some areas the cells with differences between −0.007 and 0 m and the ones with differences between 0 and 0.005 m are located in close vicinity of each other. Hence, for these areas the colors yellow and light blue are mixed and appear green.

The importance of these differences is to be assessed from a statistical point of view, that is, whether the difference between the median and mean is statistically significant (meaningful), and hence null and alternative hypotheses are considered

Table 2. Characteristics of Norbit WBMS and Kongsberg EM 3002D in the dual-head configuration used in Areas A and B, respectively

	MBES	
Parameter	Kongsberg EM 3002D	Norbit WBMS
Maximum number of soundings per ping	508	512
Beam spacing mode	Equidistant	Equidistant
Maximum swath width (degrees)	200	160
Along-track opening angle (degrees)	1.5	1.9
Across-track opening angle (degrees)	1.5	0.9
Maximum ping rate (Hz)	40	60

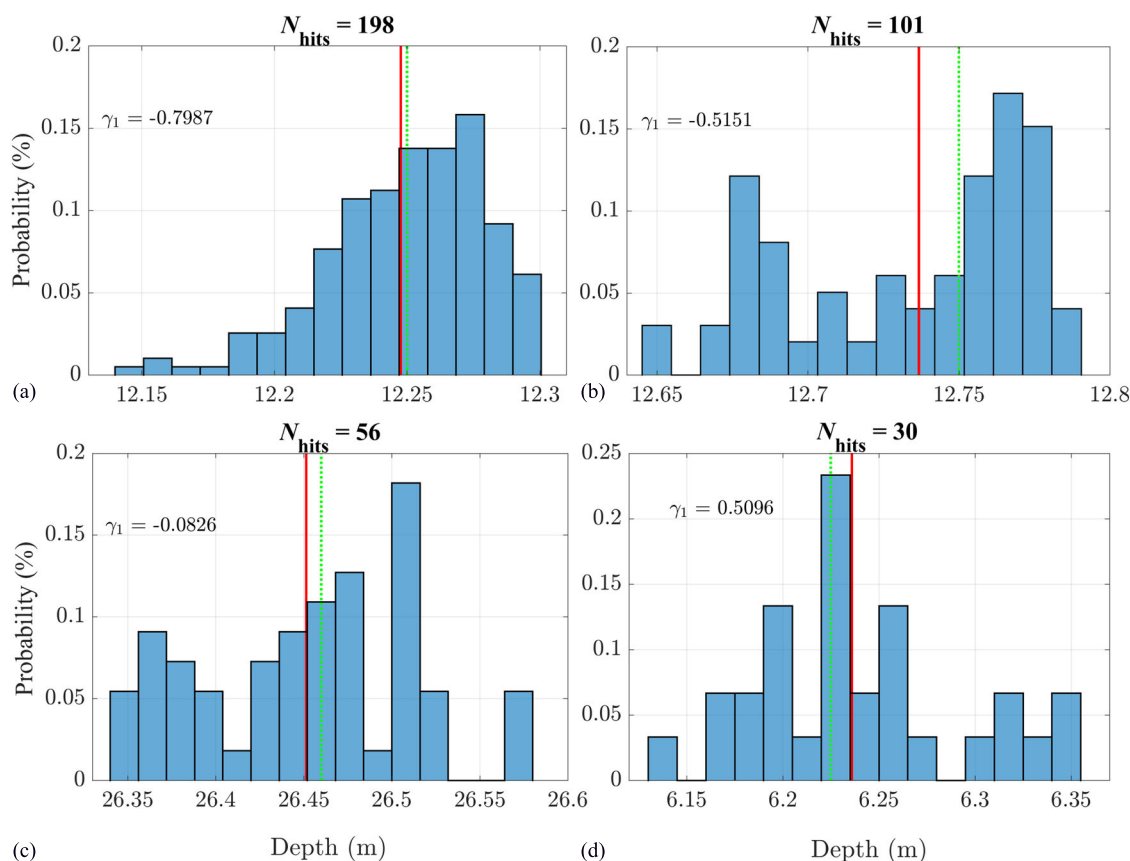Sources: Data from Norbit (2010); Kongsberg (2006).

Fig. 2. (Color) Distribution of the depth measurements within four cells with (a) 198; (b) 101; (c) 56; and (d) 30 soundings. The vertical solid line indicates the median, whereas the dotted line indicates the mean depth. Symbol γ_1 indicates the skewness.

$$\begin{cases} H_0 & : E(\underline{x}) = 0 \\ H_1 & : E(\underline{x}) \neq 0 \end{cases} \qquad (9)$$

where $\underline{x}$ = variable (difference between mean and median). If H_0 is rejected, it means that the expected value of the variable is statistically significant. Hypothesis testing is usually carried out using the probability density function (PDF) of a random variable. However, here the PDF of the variable is not theoretically known (it varies from cell to cell), and hence one may use Chebyshev's inequality (Teunissen et al. 2006), which avoids distributional assumptions for

the random variable. However, the bounds provided are quite conservative. Chebyshev's inequality states that for a random variable ($\underline{x}$) with $\bar{x}$ and $\sigma_{\underline{x}}$ being its mean and standard deviation, respectively, the following holds for every m:

$$P(|\underline{x} - \bar{x}| < m\sigma_{\underline{x}}) \geqslant 1 - \frac{1}{m^2} \qquad (10)$$

Thus, the probability masses outside the interval $(\bar{x} - m\sigma_{\underline{x}}, \bar{x} + m\sigma_{\underline{x}})$ are smaller than $1/m^2$ for every m regardless of the form of the PDF of $\underline{x}$. Therefore, under the null hypothesis, the 95% confidence interval is obtained for $m = 4.47$, indicating that $-4.47\sigma_{\underline{x}} \leqslant \bar{x} \leqslant 4.47\sigma_{\underline{x}}$. The bounds provided by Chebyshev's inequality are quite conservative; as an example, the 95% confidence interval is larger than the case with a normal distribution. This means that if the null hypothesis is rejected using Chebyshev's inequality, it will indeed be rejected for an arbitrary distribution. However, the reverse situation does not necessarily hold, that is, if $\bar{x}$ is within the bounds of Chebyshev's inequality, one cannot state that the difference between the mean and median is not significant for an arbitrary distribution. For the case under consideration, with the mean and standard deviation of the difference between the mean and median equaling -0.001 and 0.015 m (the null hypothesis is not rejected), one can only state that there is no evidence of the mean and median being different from a statistical point of view. Finally, from Fig. 3 it is seen that the differences tend to show a stripy behavior. This will be discussed in more detail in the following section. A similar study was carried out, comparing the differences between standard deviation and MAD, indicating that the standard deviation can be used as a measure for the data variability. A similar conclusion was drawn from the comparison between mean and median and standard deviation and median absolute deviation of the surveyed Area B.
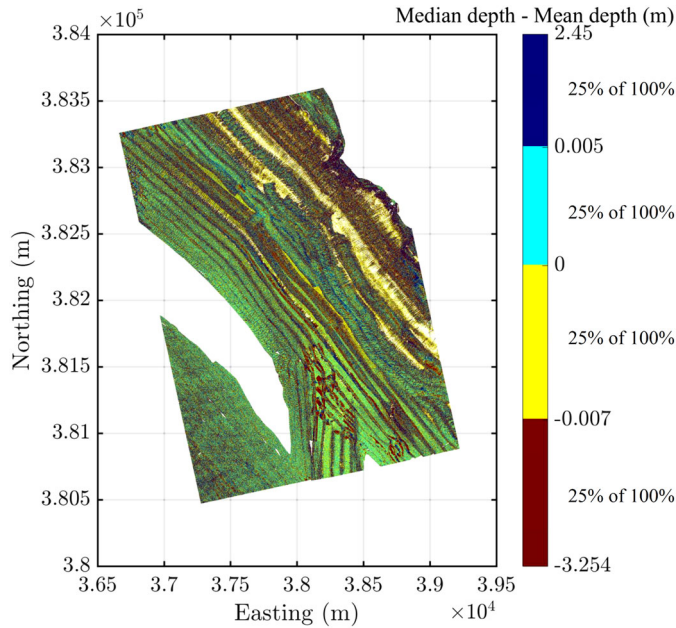

Fig. 3. (Color) Map of the difference between the median and mean depths for Area A. The range of values represented by each color is such that each range represents an equal percentage of the data.

Use of the Mean Instead of the Shallowest Measured Water Depth

Figs. 4(a and b) show the difference between the mean depth and the shallowest depth per cell for Areas A and B, respectively. The
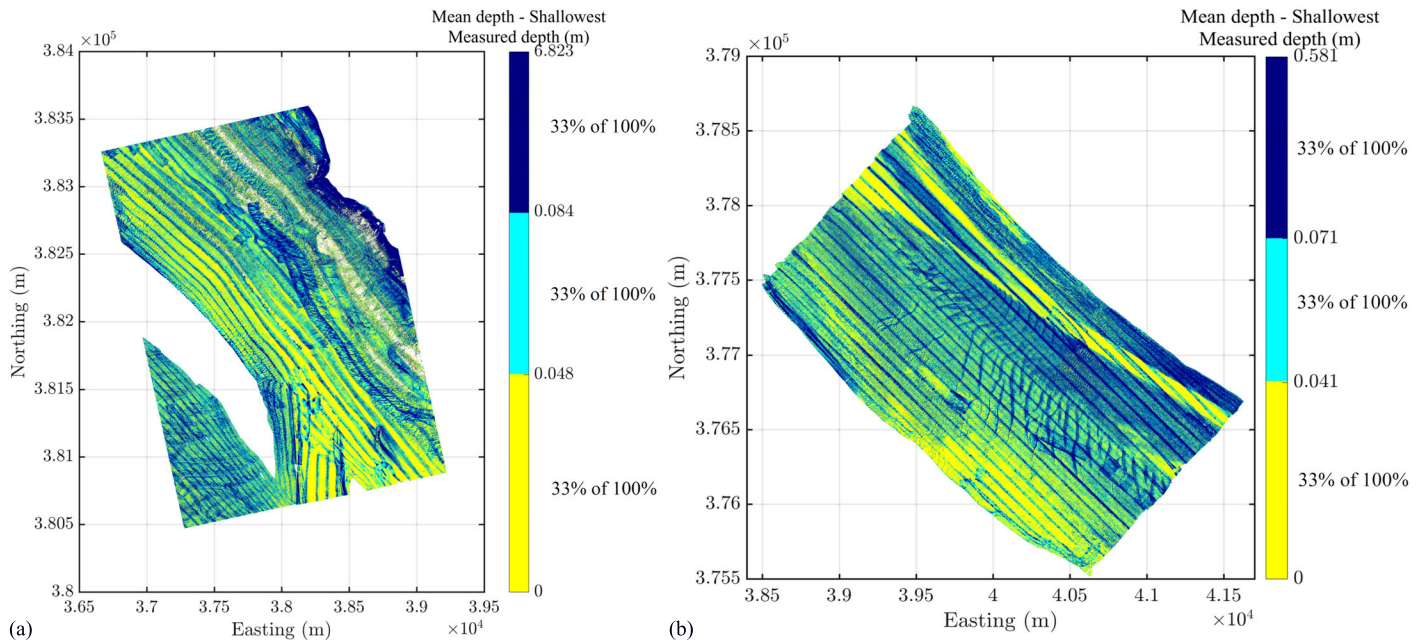

Fig. 4. (Color) Maps of the difference between the mean and shallowest depth (a) for Area A; and (b) for Area B. The range of values represented by each color is such that each color represents an equal percentage of the data.
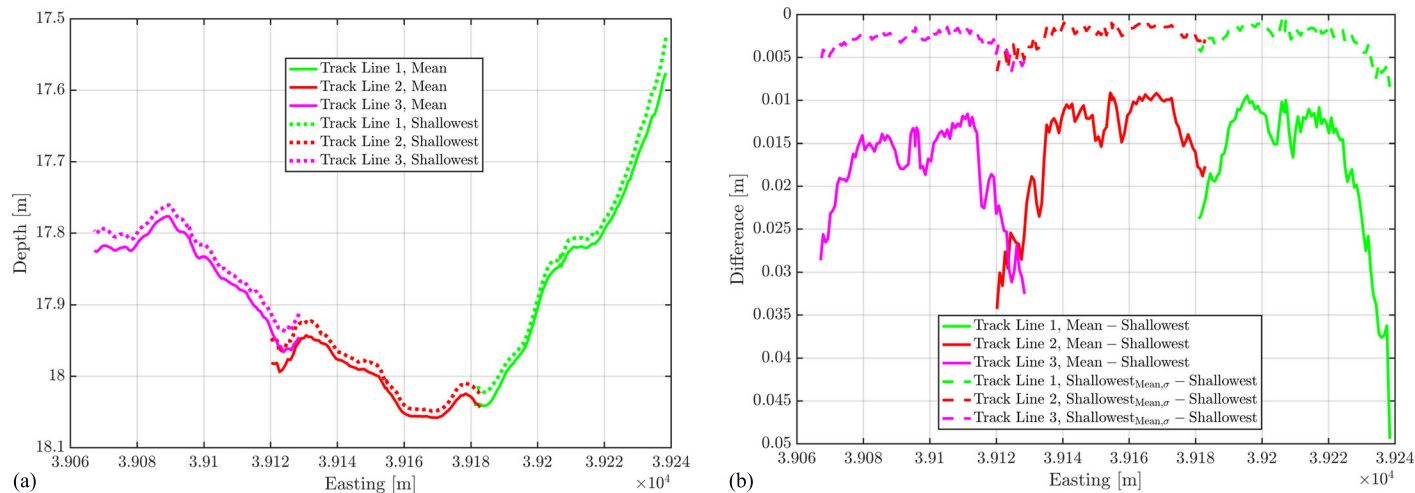
Fig. 5. (Color) (a) Mean (solid) and shallowest (dotted) depths for a small area within Area B indicated by the black rectangle in Fig. 1 consisting of three track lines; and (b) the difference between the mean and shallowest depths (solid) and the difference between the mean, corrected for standard deviation, and shallowest depths (dashed).

maximum absolute difference between the mean and shallowest depth in Fig. 4(a) (6 m) is significantly larger than that of Fig. 4(b) (0.6 m). Fig. 4(a) clearly demonstrates the need for improved mapping compared to using the shallowest measured depth per cell because it is considered impossible to have a 6-m difference between the shallowest and mean depth in a 1×1 m^2 cell. In addition, the results show a dependency along the sailing direction. This dependency, which was not observed in the bathymetry, exists irrespective of the topography and type of the MBES employed and the difference between the two depths gradually increases from nadir to the outer beams. To closely examine the origin of this dependency, the seafloor profiles for both a flat area and a nonflat area were considered.

Shown in Figs. 5(a and b) are the mean and shallowest depths, obtained as an average over nearly 150 pings, and the difference (solid lines) between these two for a relatively flat area [indicated by the black rectangle in the bathymetry map Area B (Fig. 1)]. It is seen that this difference increases toward the outer parts of the swath [Fig. 5(b)], resulting in the dependency observed. It is hypothesized that this increase is due to the fact that the uncertainties inherent to the MBES, due to uncertainties in, for example, roll and steering angle, increase toward the outer parts of the swaths (i.e., with an increase in the beam angle) (Lucieer et al. 2016; Maleika 2013). The shallowest depth measured per grid cell is more affected by these uncertainties than is the mean depth. This is due to the fact that no averaging is used for the first. The value of 0.01 m, corresponding to measurements directly underneath the MBES, can thus be considered to represent, at least for the considered part of Area B, the minimum value of the expected change in estimated water depth (getting deeper) when instead of the shallowest depths, mean depths are presented for flat areas.

An interesting point to address here is the effect of an increase in the cell size. Shown in Fig. 6 are the same parameters as shown in Fig. 5(b) with the cell size of 4×4 m (instead of 1×1 m). As shown, the coarser grid does not hamper observing the increase in the differences toward the outer part of the swaths (larger beam angles). However, as expected, the level of detail that was observed in Fig. 5(b) has decreased. As for the effect of cell size on the shallowest and mean depth representatives, the former gets shallower when the cell size increases because the shallowest depth is assigned to a larger area. While having a smaller cell size theoretically increases the depth estimate based on the shallowest measured
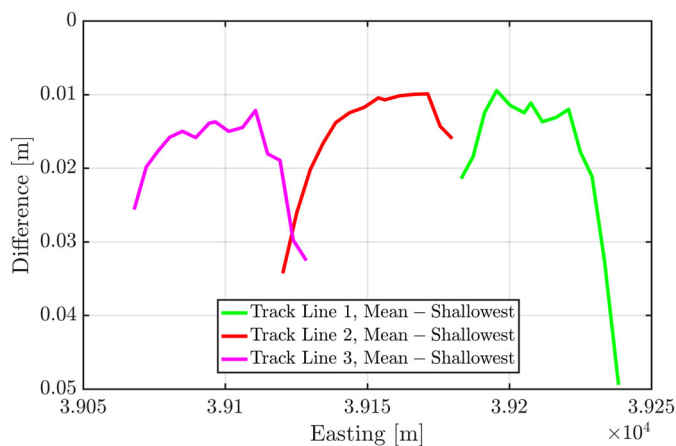

Fig. 6. (Color) Difference between the mean and shallowest depths for the same area shown in Fig. 5 with four times larger cell size than that of Fig. 5(b).

depth, it does not change the depth estimate derived from the mean to a noticeable extent. However, one should take the MBES along- and across-track resolutions into account when choosing a cell size. A more advanced alternative to the fixed-resolution gridding is the multiresolution grid. This leads to data compression depending on the bottom morphology and enables one to capture the variability of the beam footprint and the data density; see as an example Maleika et al. (2018) and Debese (2007). One can also relate the patches together, leading to a smooth surface approximation. This can be done using the theory of polynomial spline approximation. A spline function is a piecewise polynomial interpolation such that these polynomials are joined together under some continuity conditions; see as an example Amiri-Simkooei et al. (2018) and Zangeneh-Nejad et al. (2017). However, because this is susceptible to introducing unwanted depth variations, this approach is more suitable for morphological studies (where focus is on specific bathymetric features) and not for charting purposes (where the safe navigation is of importance) as considered in this paper.

Generally speaking, the degradation in quality of the MBES bathymetric measurements is not solely due to the uncertainties

inherent to the MBES; various other error sources can be considered. One of the contributors is the systematic error sources, which can be categorized as static and dynamic. The former includes (but is not limited to) the relative heading, pitch, and roll misalignments between the MBES and the INS and the relative time missynchronization between the positioning sensor and the MBES clock [see Godin (1998) for a detailed discussion on the various systematic error sources]. As an example, the roll offset induces a depth error that increases with the beam angle, and hence its signature is similar to the one observed. Therefore, it is important to properly take them into consideration to avoid any misinterpretation. The correction of the previously mentioned static systematic sources is done using the patch test, which examines the repeatability of the system over a predefined patch of the seafloor. For both surveyed areas, the patch test was carried out, and therefore these systematic errors (if present) have been excluded. The other type of systematic errors are dynamic and produce errors that vary either with periods in the ocean wave spectrum or with a long period acceleration of the vessel (Hughes Clarke 2003). These errors can be identified using the correlation analysis between the motion time series and depth derivatives. Both data sets have been examined carefully and the signatures of the dynamic systematic errors have not been found. Another error source with a signature similar to that observed (increase toward the outer parts of the swath) is the SSP. Using an erroneous SSP induces errors in the estimate of both the depth and beam steering, resulting in the under- or overestimation of the depth for the outer beams, and hence depth artifacts referred to as *smile* or *frown* are observed in the bathymetry map (Dinn et al. 1995). This error can be identified using the overlap between the adjacent swaths. Considering the fact that the time interval between the measurements of the adjacent lines for both surveyed areas is maximally up to several hours, the bottom features such as megaripples and sand dunes do not vary within this relatively short period. Therefore, the depths as determined from the measured travel times along two overlapping swaths should be the same at equal points on the seafloor. Using an erroneous sound speed profile results in discrepancies between these measurements (Snellen et al. 2009). A careful assessment of the footprints' depth at the overlapping parts for both surveyed areas over different parts (flat and nonflat) confirmed that the correct sound speed profiles were used. Therefore, it was concluded that the observed increase in the differences toward the outer parts of the swath were not caused by systematic error sources.

To further investigate the validity of the hypothesis that for the flat area the difference between shallowest and mean depth is caused by the MBES measurement uncertainties, a model for predicting the measurement uncertainties was used. Fig. 7 shows the predictions for the vertical uncertainties induced by different error sources inherent to the MBES for the water depth of around 18 m. This prediction was obtained from the model A priori Multibeam echo sounder Uncertainty Simulation Tool (AMUST). The equations used were based on Hare (1995) and the uncertainty sources considered were the range measurements, roll and steering angle, pitch angle, along-track opening angle, sound speed profile, and heave. The term describing the error in the range measurements is often considered to result in predicting too-high uncertainties (Hare 2001). Therefore, this term was scaled by 0.707 compared to Hare (1995). The total uncertainty was derived as the square root of the sum of the square of individual sources (assuming they are independent) (solid cyan curve in Fig. 7). Also shown in Fig. 7 is the standard deviation of the depth measurements (blue dashed curve with triangles). A total of 150 pings were used to calculate this standard deviation. The comparison between the modeled and measured uncertainties shows good agreement in both the order of magnitude as well as in the behavior of the uncertainties with beam angle. Both the model and the measurements indicate increasing uncertainties with increasing beam angle, reflected in the stripes as observed in Figs. 4(a and b). Discrepancies between AMUST predictions and measurements can at least partly be explained by the presence of some bottom features. Although the approaches presented in this contribution are not based on a priori estimates of the depth uncertainties, there are approaches that do need this estimate as an input, such as CUBE, and hence a realistic estimate of this parameter is required. The agreement between the modeled and measured uncertainties indicates that indeed the model can capture the measured standard deviation.
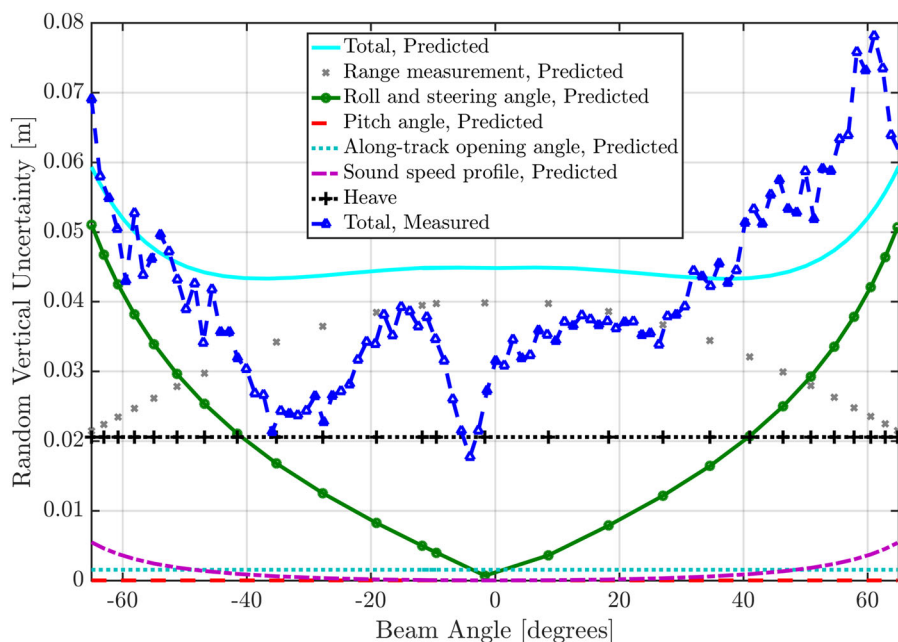

Fig. 7. (Color) Total random vertical uncertainty predicted (cyan curve) due to the contribution of individual error sources inherent to the MBES along with the measured uncertainty from the bathymetry measurement (blue dashed curve with triangle markers) for Track Line 3 in Fig. 5.
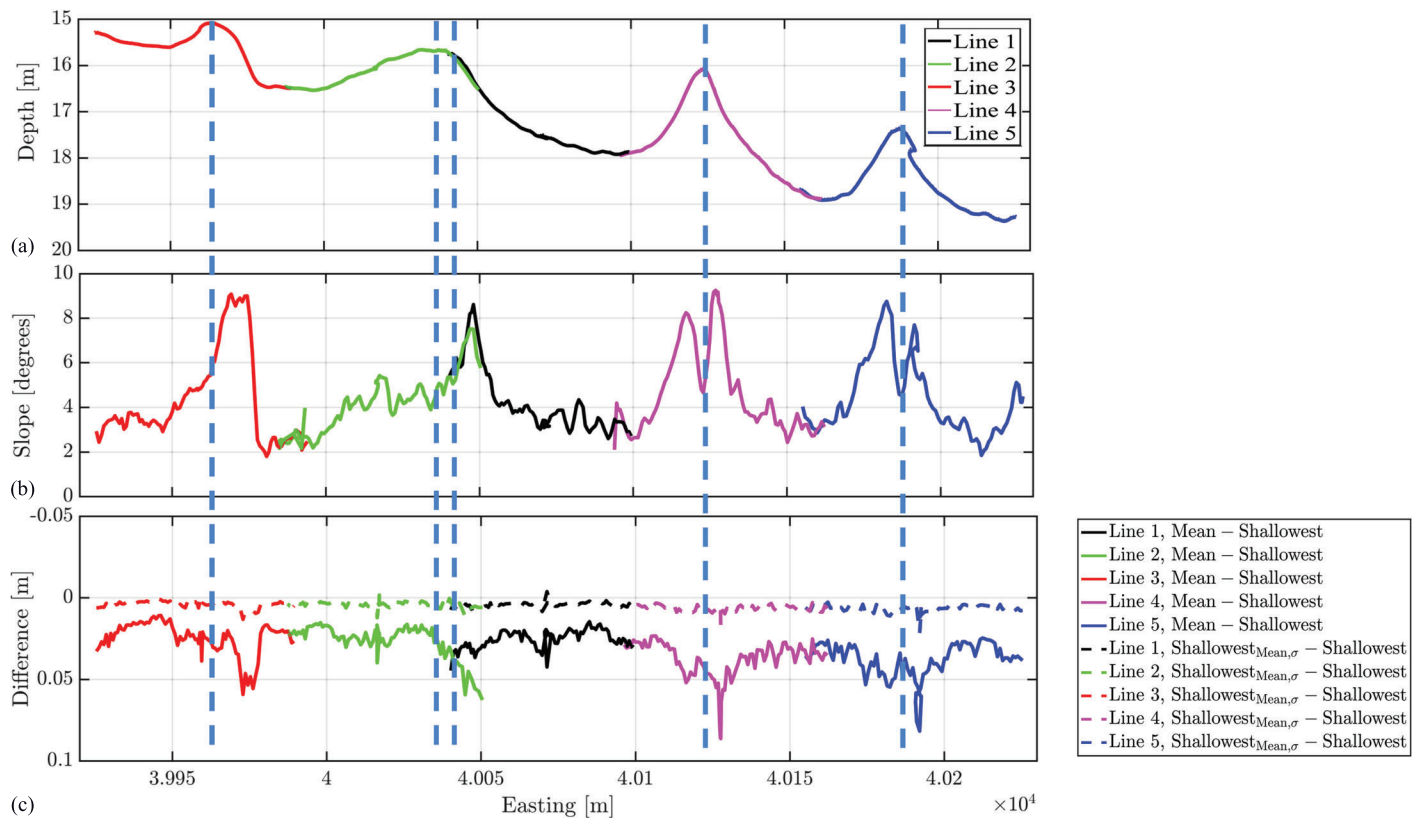
Fig. 8. (Color) (a) Mean depth; (b) mean slope; and (c) mean difference between mean and shallowest depths (solid) and mean difference between mean and standard deviation and shallowest depths (dashed) for the black area indicated by the black dashed line shown in Area B in Fig. 1. This area consists of five track lines and nearly 30 pings. The blue dashed vertical lines indicate the location of the shallowest depth for each swath.

It can be concluded that for flat areas, using the shallowest measured depths results in mapping depths that are affected by measurement uncertainties. It is known that these uncertainties in the measurements change with beam angle, water depth, and measurement equipment (Maleika 2013), as an example. Thus, the magnitude with which the uncertainties affect the mapped depths will be location and survey dependent.

Regarding the nonflat regions, a small area consisting of five track lines and 30 pings was considered (black dashed area in Fig. 1). A small number of pings were chosen to ensure that the topography does not change. For each ping, the measurements were averaged over five beams and the profile for mean depth [Fig. 8(a)] was derived by averaging over the 30 pings for each track. From Fig. 8(c) it is seen that now, in contrast to the flat area, the larger differences between mean and shallowest depth do not occur at the outer parts of the swaths. In this case the largest differences are found at the locations of morphological features. Specifically, it is seen that the maximum differences occur at regions with larger slopes [Fig. 8(b)], as expected for a sloping plane. To further assess the correlation between the differences and the slopes, these two parameters along with their linear fit are shown in Fig. 9, indicating increasing differences between the mean and shallowest depths with an increase in the slope (correlation coefficient between the two parameters is 0.624, which is significant at the 95% confidence level). As discussed, an increase in the cell size leads to a less-detailed seafloor representation. This affects the nonflat regions to a larger extent than that of the flat regions because larger depth variations are expected in a small area [see Figs. 10(a and b), where the same parameters as shown in Figs. 8(b and c), respectively, are presented for a four times larger cell size]. Take Line 3 (red) as an
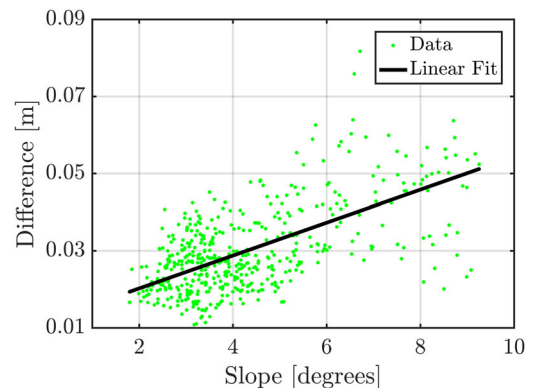

Fig. 9. (Color) Mean slope versus mean differences for the black dashed area shown in Area B in Fig. 1 (points) and its linear fit (line).

example, from Fig. 8(b) (1-m cell size): the slope at the beginning of the swath is not very steep; however, if the cell size decreases, one might interpret it as a steep slope. Similar to the flat areas, having a coarser grid for the nonflat regions results in a shallower grid compared to that of the fine grid; however, the magnitude of the change is larger than that of the flat areas.

Based on the preceding, it is concluded that for flat areas, the differences between mean and shallowest measured depths are dominated by the MBES measurement uncertainties. These result in depths that are shallower than the actual shallowest depths, with the magnitude of the offset varying along the MBES swath. For nonflat areas, an additional contribution is due to the presence of slopes that
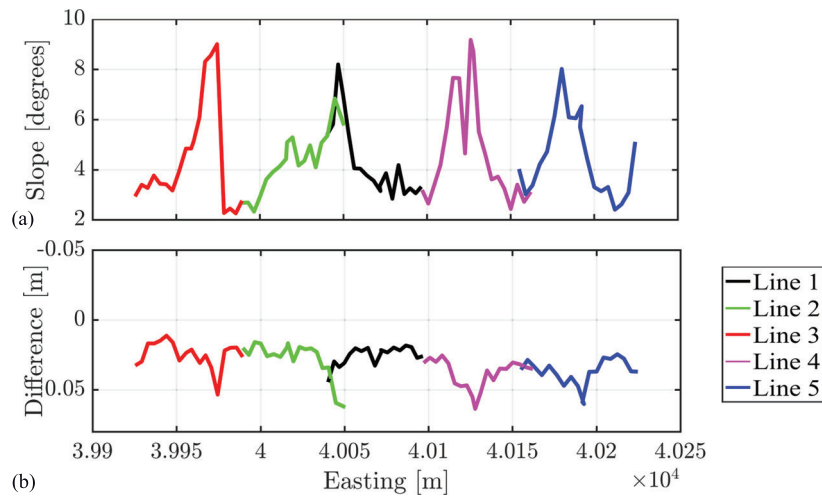
Fig. 10. (Color) (a) Mean slope; and (b) mean difference between mean and shallowest depths for the same area shown in Fig. 8 with four times larger cell size than that of Figs. 8(b and c).
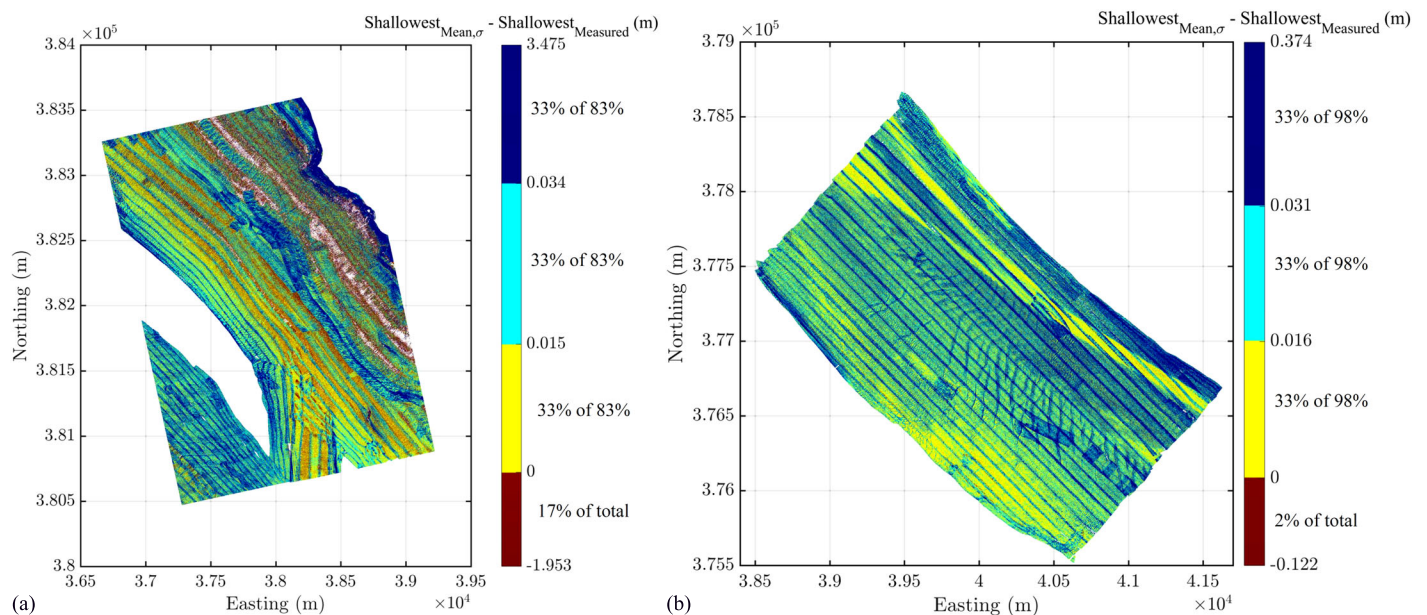

Fig. 11. (Color) Maps of the difference between the shallowest depth based on the mean plus standard deviation and the shallowest depth measured (a) for Area A; and (b) for Area B. The positive range of values represented by each color is such that each color represents an equal percentage of the data for which the derived depths are deeper than the shallowest measured depths. Dark red indicates those data points where the derived depths are shallower than the shallowest measured depths.

inherently results in a difference between the mean and shallowest depth in a cell. While the effect of measurement uncertainties can be counteracted by using the mean instead of shallowest depth, this will result in an overestimation of the depth in nonflat areas, that is, it gets deeper. Considering the importance of guaranteeing safe navigation, this can be considered as an undesirable situation. Indeed, assigning a realistic depth value in nonflat regions where steep slopes exist is an issue of great interest and has been discussed by various scholars. Vásquez (2007) found that for areas with extreme seafloor morphology and steep slopes, even the advanced surface estimation approaches, such as CUBE, might fail to provide a realistic and robust estimate of the depth. Modification of the different CUBE parameters resulted in a more realistic surface representation. The irregular and nonflat bottom can also complicate the iden-

tification and rejection of the outliers and automatic data cleaning approaches might not be applicable [see Artilheiro (1998) for a detailed discussion]. These steep slopes, however, are not encountered on the Dutch continental shelf, the focus area of this study.

Shallowest Depth Based on the Mean and Standard Deviation

To account for the overestimation of the depth in nonflat areas, Eq. (1) was used. Shown in Figs. 11(a and b) are the maps of the differences between the shallowest depth based on the mean and standard deviation and the shallowest measured depth per cell for Areas A and B, respectively.

Different color bars are used for the two areas for representing

the difference between the shallowest depth derived (i.e., using the standard deviation) and the one measured. For decreasing difference between the mathematical shallowest depth and the shallowest measured depth while being positive, the color gets lighter. The range of values for each color was selected such that each color represents a certain percentage of all data points (33% here). Dark red in Fig. 11 indicates that the resulting depth is shallower than that actually measured. For 17% of the cells in Area A, the shallowest depth based on the mean and standard deviation is up to 1 m shallower than the shallowest depth measured (only for 0.002% of the cells does the difference exceed 1 m). Regarding Area B, the range of the differences is considerably smaller and for a smaller percentage (around 4%) of the cells the shallowest depth derived is shallower than the one measured. Obtaining a shallower representative than the shallowest measured depth indicates that the standard

deviation within a cell is larger than the difference between the shallowest and mean depths [Eq. (1)]. This phenomenon, which is somewhat unexpected, can be explained by the fact that the distribution of depth values within a cell does not necessarily need to be symmetrical (Figs. 2 and 3) and can be skewed. The standard deviation does not reflect this asymmetry in the distribution, resulting in derived depths that are shallower than the actual shallowest depth.

To investigate in more detail the effect of using this measure in a flat area, the dashed lines in Fig. 5 show the difference between the shallowest measured depth and the approach considered in this section. For the tracks considered, it is seen that the estimated depths are larger than those obtained when taking the shallowest depth. Also, the standard deviation is affected by the MBES measurement uncertainties, as is the shallowest measured depth. However, since the effect is smaller for the standard deviation than for the minimum, Fig. 5 shows a less pronounced dependency along the swath compared to Fig. 4. More interesting is the effect of using the measure for depth as considered in this section for an area with slopes. The results are shown in Fig. 8(c) as the dashed lines. From this figure it is seen that now the slopes no longer significantly contribute to the difference. The difference at the locations of the slopes is now comparable to those found for the remaining locations.

Based on the preceding discussion, it can be concluded that although using the combination of mean and standard deviation results in estimates for the water depth for flat areas that are close to those corresponding to the shallowest measured depth, that is, underestimating the actual depth, the standard deviation seems an appropriate way to account for the presence of slopes.

Table 3. Depth values at four corners of the cell in Area A with parameters as presented in Table 4

Corner	Depth (m)
Upper left	10.78
Lower left	46.78
Lower right	78.12
Upper right	42.12

Note: Depth is considered positive downward.

Table 4. Easting and northing of the cell center along with mean depth, number of soundings, slope angles, and regression coefficients for a cell in surveyed Area A with unrealistic depth values at the corners

Parameter	Value
Easting (m)	38,846.5
Northing (m)	382,065.5
Mean depth (m)	44.45
N_{hits}	7
Slope angle (degrees)	88.8
Slope direction (degrees)	318.96
C_X	−31.34
C_Y	36.00

Note: Depth is considered positive downward.

Mathematical Shallowest Depth Based on the Regression Coefficients

The shallowest depth based on the regression coefficients was derived using Eq. (8). Theoretically, this measure is a highly realistic representation of the shallowest depth in a cell because the effect of potential slopes is fully taken into account by calculating the shallowest depth at the corner. It was, however, found that when applying this method to the MBES point cloud data, unrealistic depth values were obtained for some cells, in agreement with Mohammadloo et al. (2018). As an example, consider the four depths derived for the corners of a cell in Area A (Table 3). Considering the
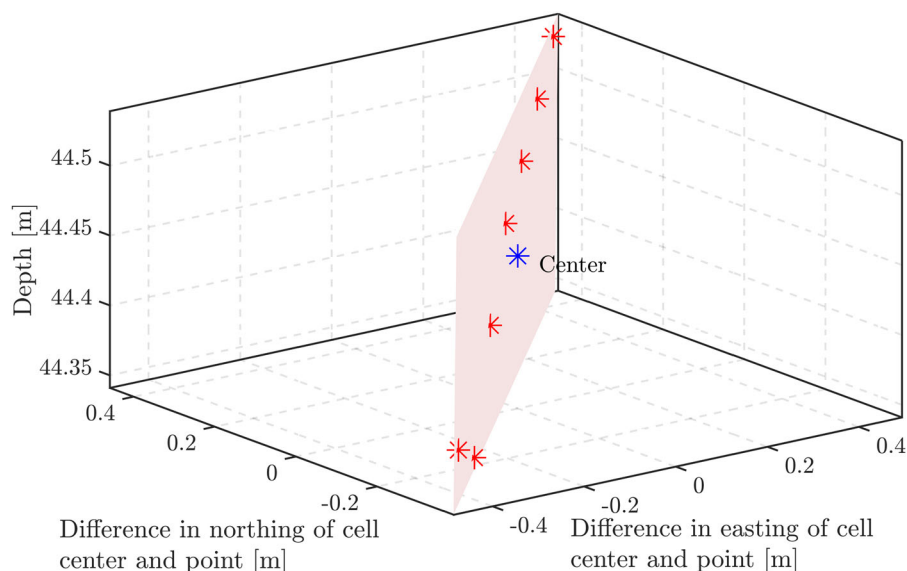

Fig. 12. (Color) Distribution of the points in the cell (red) with the center (blue) coordinates presented in Table 4 (Area A) along with the fitted plane.

mean for this cell (44.45 m, Table 4) and the cell size 1 m², it is almost impossible to obtain a depth of 10.78 m as the shallowest depth at the upper-left corner. To understand the reason behind obtaining the unrealistic depth values at the cell corners, the distribution of the soundings within a cell having this issue was assessed.

Table 4 presents the coordinates of the cell center, mean depth, number of soundings, regression coefficients, and slope angles for a cell in Area A with depth values at the corners as shown in Table 3. Fig. 12 illustrates the distribution of the soundings in this cell. It is seen that the points are not well distributed within the cell under consideration, and hence the design matrix (A) is badly invertible.

As a result, the coefficients should only be used to determine the depth in the vicinity of the points rather than at the corners of the cell (Mohammadloo et al. 2018). The problem can be addressed by computing the condition number of the normal matrix ($A^{T}A$) of size 3×3 (Press et al. 1992) as done by Biagi and Carcano (2015). The eigenvalue decomposition of the positive definite normal matrix is

$$A^{T}A = U\Lambda U^{T} \qquad (11)$$

where $\Lambda = \mathrm{diag}(\lambda_{11}, \lambda_{22}, \lambda_{33})$ is a diagonal matrix with diagonal entries the eigenvalues of $A^{T}A$; and U is a 3×3 matrix of eigen-
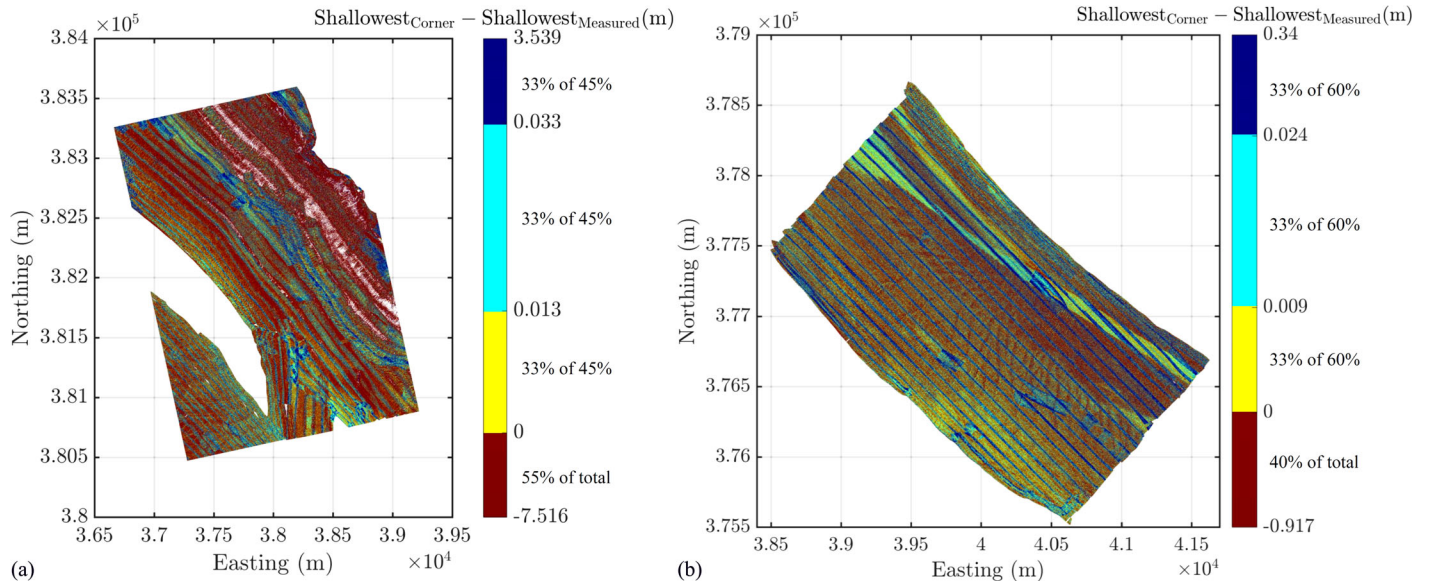

Fig. 13. (Color) Maps of the difference between the shallowest depth at the corner of the cell (based on regression coefficients) and shallowest depth measured for (a) Area A; and (b) Area B. The positive range of values represented by each color is such that each range represents an equal percentage of the data for which the derived depths are deeper than the shallowest measured depths. Dark red indicates those data points where the derived depths are shallower than the shallowest measured depths.
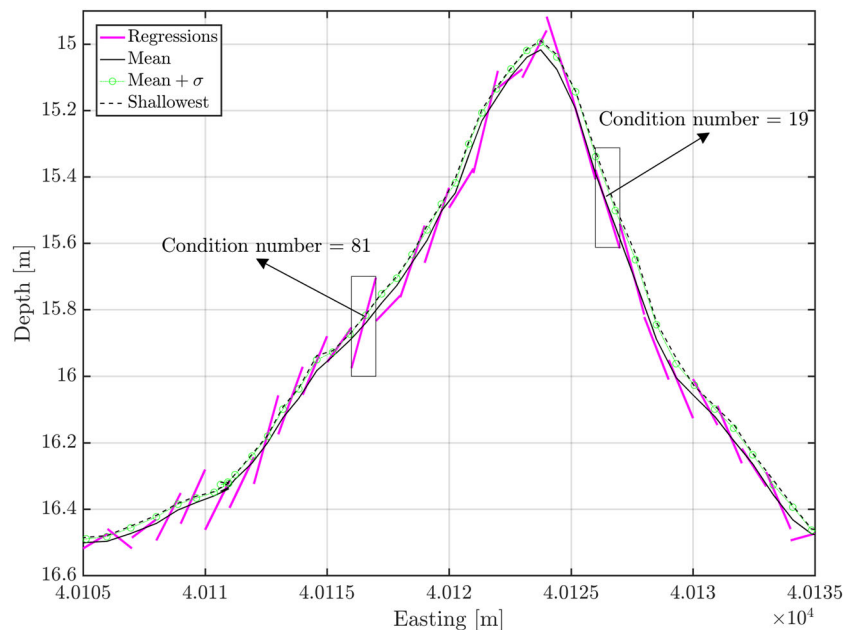

Fig. 14. (Color) Depths using mean (solid black), mean and standard deviation (dotted green with circle), and shallowest measured (dashed black) along with the linear regressions (magenta). The rectangles indicate two cells with large and small condition numbers.

vectors where each column corresponds to one of the eigenvalues, $\lambda_{ii}, i = 1, 2, 3$, of the normal matrix. If the matrix $\boldsymbol{A}^T\boldsymbol{A}$ is singular or ill conditioned, some of the eigenvalues are (almost) zero. The condition number, which is defined as the ratio of the largest (in magnitude) eigenvalue to the smallest eigenvalue, will thus take large values. For Areas A and B, the condition number exceeds 10^2, 10^3, and 10^5 in 5%, 3%, and 2%, and 0.1%, 0.07%, and 0.02% of the cells, respectively. For the research presented here, cells with the condition number larger than 10^2 were excluded from the analysis and their eight neighboring cells have been used to assign the required parameters (such as regression coefficients) for these cells.

Shown in Figs. 13(a and b) are the differences between the shallowest depth based on Eq. (8) after excluding the badly conditioned cells and the measured shallowest depth in a cell for Areas A and B, respectively. It is seen that for around 55% and 40% of the cells in Areas A and B, respectively, the depth derived is shallower than its measured counterparts. For nearly 95% of the cells in Area A for which the depth derived is shallower than the one measured, the differences are less than 0.2 m. As for Area B, for around 99% of these cells the differences are less than 0.1 m. This means that the largest differences shown in the color bars (7.516 and 0.917 m for Areas A and B, respectively) occur for a negligible portion of the cells.

To further investigate the performance of the approach based on the regression coefficients, an area consisting of one track line (on a slope) and six consecutive pings was considered (covering 1 m along the sailing direction). For each ping, the measurements were averaged over five beams. Shown in Fig. 14 are the linear regressions along with the estimate of depth based on the mean, mean and standard deviation, and shallowest measured. For a large number of cells, the best fitted planes show a discontinuous and unrealistic representation of the seafloor. As explained, the unrealistic estimate of the regression coefficients is due to the distribution of the soundings within the cells (Fig. 12), resulting in a relatively large condition number (such as the condition number of 81 shown for the cell in Fig. 14). In a small region, right of the peak, a more continuous representation of the bathymetry as derived from the regression coefficients per cell is found. For this area, lower values of the condition number are found. This result indicates that the applicability of the approach based on the regression is highly sensitive to the distribution of the measurements. Consequently, employing it is not encouraged. One approach to minimize the negative effect of outliers and to decrease the sensitivity of the this method to the distribution of the points is to calculate the regression coefficients for a local $N \times N$ window of the cells instead of a single cell; however, this will result in a grid with varying cell size (i.e., multiresolution), which was not considered in the present contribution.

The average values of the depth based on the mean and standard deviation, regression coefficients, mean, and the shallowest measured depth for both surveyed areas are shown in Table 5. The deepest and shallowest representatives are based on the mean and the regression coefficients, respectively. The averaged value of the depth based on the mean and standard deviation is between those based on the shallowest measured and mean depths.

The different approaches presented in this paper for the estimate of the depth are not to be viewed as a replacement for the more sophisticated methods, such as CUBE [developed by Calder and Mayer (2001)]. However, the fact that they do not require a priori estimate of the depth uncertainties (i.e., they are based on the statistics from the soundings) and are simple to implement (particularly the depth estimate based on the mean, shallowest, and mean plus the standard deviation) make them appropriate alternatives in case detailed information of the soundings uncertainty is not available. Nevertheless, the depth estimates derived using the shallowest, mean, mean and standard deviation, and regression coefficients were compared to that of the CUBE implemented in Qimera processing software (developed by QPS) to give an insight into their agreement

Table 5. Average value of the shallowest measured, mean, and mathematical shallowest depths for surveyed areas A and B

Various depth representatives	Surveyed area	
	A	B
Shallowest measured depth (m)	24.87	14.92
Shallowest depth based on mean and standard deviation (m)	24.89	14.95
Shallowest depth using regression coefficients (at the corner) (m)	24.85	14.91
Mean depth (m)	24.94	14.99

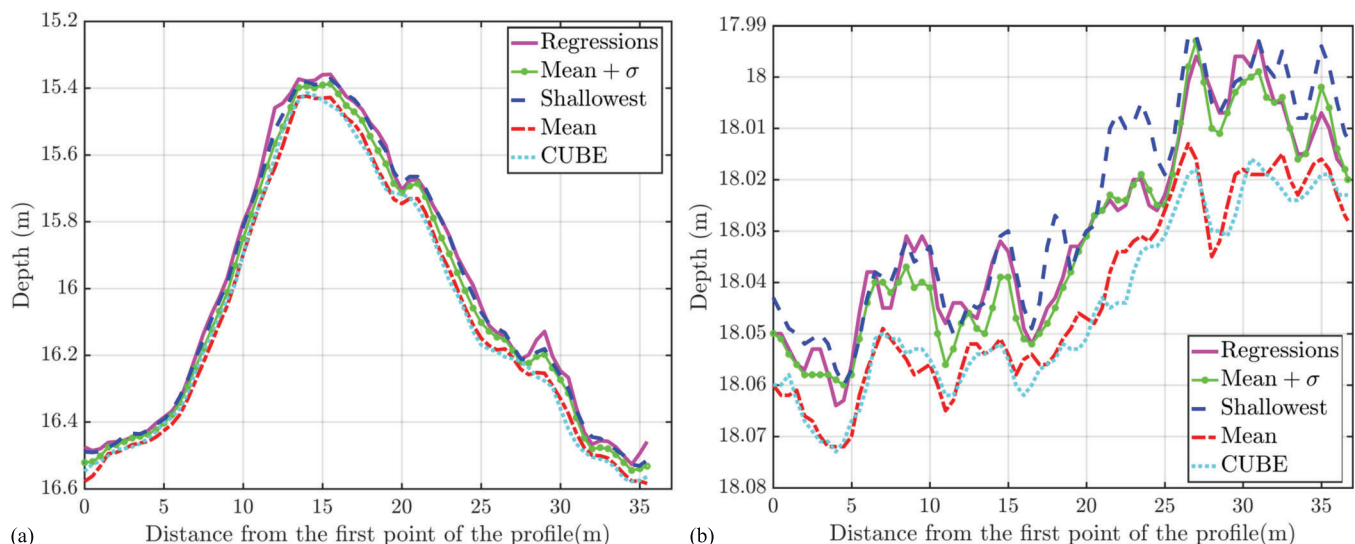Note: Depth is considered positive downward.

Fig. 15. (Color) Depths using mean (dashed red), mean and standard deviation (solid green with circles), and shallowest measured (dashed blue), regression coefficients (magenta) along with the CUBE (dotted cyan) estimate for (a) nonflat; and (b) flat parts.

and possible discrepancies. For CUBE processing, the default Qimera configuration for shallow water was chosen, which contained the parameters suitable for areas where small-scale features are important. Information on the parameters used in Qimera can be found in Penney (2018), and an interested reader might also refer to Calder and Wells (2007) for a detailed description of CUBE. The comparison was carried out for two parts of the seafloor, in nonflat and flat areas. Both parts were chosen such that they correspond to the data for small beam angles. Regarding the nonflat part, an across-track profile of length 35 m in the area indicated by a dashed line in Fig. 1 was chosen. Fig. 15(a) illustrates the depths obtained using different approaches. The estimate of CUBE is in a good agreement with that of the mean. This indicates that using CUBE for the slopes with the default settings in Qimera results in an overestimation of the depth (getting deeper) and therefore the method based on the mean and standard deviation seems to give a more realistic estimate. Regarding the seafloor profile for a flat part [Fig. 15(b)], the CUBE estimates again closely follow the mean depth. This is somewhat expected because for a flat seafloor with randomly distributed soundings with comparable uncertainties (as the inner part of the swath is considered), the mean depth is close to output of the Kalman filter.

Conclusion

The MBES provides a nondestructive and cost-effective way to produce qualitative and quantitative bathymetry maps. The resulting MBES point cloud data contain millions of soundings and are, in general, not directly used for charting. A straightforward approach for equidistance gridding, often adopted, is to consider the shallowest depth at the center of the cell. The grids derived can be artificially shallow due to the presence of erroneous soundings. An approach to address this issue is to use the mean depth instead. However, this may lead to not charting hazardous objects imperative for safe navigation. In this paper, approaches to derive depths from the point cloud (in addition to mean and shallowest depths) using the statistical properties of the point cloud are proposed and applied to two different surveyed areas within the Netherlands that are important because they contain critical locations important for shipping. Based on the results, the following conclusions are drawn.

Two issues were found to be of importance for the quality of the resulting estimates for shallowest depth: the distribution of the soundings over a cell and the MBES measurement uncertainty. While a proper distribution of the measurement points within a cell is crucial for the approach based on the regression coefficients, the approach using the mean depth together with the standard deviation requires minimum uncertainties in the depth measurements. For the surveys considered, the distribution of MBES measurements hampered a proper estimation of the slopes and thus negatively affected the estimates for shallowest depths based on the regression coefficients. Using the mean was found to counteract the measurement uncertainties, but overestimated the depth for areas with slopes. Using a combination of the mean and standard deviation was found to capture the presence of slopes while decreasing the influence of measurement uncertainties compared to using the shallowest measured depths. These measurement uncertainties vary with beam angle, depth, and survey equipment, and can be predicted using proper modeling. This modeling can be used to select the survey strategy and potentially a subset of the full point cloud, such that there is minimum variation in the uncertainties over the area.

Another important issue to consider is the effect of the cell size on the grid derived. It has been shown that for the flat areas, increasing the cell size results in a shallower depth estimate when using the shallowest measured depth (and consequently a shallower grid is derived). The coarser grid affects the nonflat areas to a larger extent than the flat areas. This can hamper the identification of the morphological features, and hence a realistic cell size based on the depth, angular sector, number of soundings with a ping, and the vessel speed is to be chosen.

In addition, it can be concluded that the differences were found to be useful tools for identifying artifacts, but also morphological features, which are not directly observed in the bathymetry map. The morphological features can especially be of interest, for example, for seafloor sediment classification purposes. For this, often a combination of parameters derived from depth measurements and backscatter values are used for discriminating between different sediment types (e.g., Eleftherakis et al. 2012, 2014; Preston et al. 2001).

References

Amiri-Simkooei, A. R., M. Hosseini-Asl, and A. Safari. 2018. "Least squares 2D bi-cubic spline approximation: Theory and applications." *Measurement* 127: 366–378. https://doi.org/10.1016/j.measurement.2018.06.005.

AML Oceanographic. 2017. "SV and CTD profilers: Base.X2 and Minos. X." Accessed August 18, 2018. https://amloceanographic.com/wp-admin/admin-ajax.php?juwpfisadmin=false&action=wpfd&task=file.download&wpfd_category_id=117&wpfd_file_id=984&token=e7a0762935707787b9c4fddb975b6073&preview=1.

Artilheiro, F. M. F. 1998. "Analysis and procedures of multibeam data cleaning for bathymetric charting." M.S. thesis, Dept. of Geodesy and Geomatics Engineering, Univ. of New Brunswick. http://www2.unb.ca/gge/Pubs/TR192.pdf.

Biagi, L., and L. Carcano. 2015. "Re-gridding and merging overlapping DTMS: problems and solutions in HELI-DEM." In *Proc., VIII Hotine-Marussi Symp. on Mathematical Geodesy,* Vol. 142 of *International Association of Geodesy Symposia*, edited by N. Sneeuw, P. Novák, M. Crespi, and F. Sansò, 257–262. Cham, Switzerland: Springer. https://doi.org/10.1007/1345_2015_128.

Brouns, G., A. De Wulf, and D. Constales. 2001. "Multibeam data processing: Adding and deleting vertices in a Delaunay triangulation." *Hydrogr. J.* 101: 3–9.

Brouns, G., A. De Wulf, and D. Constales. 2003. "Delaunay triangulation algorithms useful for multibeam echosounding." *J. Surv. Eng.* 129 (2): 79–84. https://doi.org/10.1061/(ASCE)0733-9453(2003)129:2(79).

Calder, B. R., and L. A. Mayer. 2001. "Robust automatic multi-beam bathymetric processing." In *Proc., US Hydrographic Conf.* Rockville, MD: Hydrographic Society of America.

Calder, B. R., and L. A. Mayer. 2003. "Automatic processing of high-rate, high-density multibeam echosounder data." *Geochem. Geophys. Geosyst.* 4 (6). https://doi.org/10.1029/2002GC000486.

Calder, B. R., and D. Wells. 2007. *CUBE user's manual: Version 1.13.* Durham, NH: University of New Hampshire.

Debese, N. 2007. "Multibeam echo-sounder data cleaning through an adaptive surface based approach." In *Proc., US Hydrographic Conf.* Rockville, MD: Hydrographic Society of America.

De Wulf, A., D. Constales, T. Nuttens, and C. Stal. 2012a. "Grid models versus TIN: Geometric accuracy of multibeam data processing." In *Proc., Hydro12.* Heeg, Netherlands: Hydrographic Society Benelux.

De Wulf, A., D. Constales, C. Stal, and T. Nuttens. 2012b. "Accuracy aspects of processing and filtering of multibeam data: Grid modeling versus TIN based modeling." In *Proc., FIG Working Week 2012: Knowing to Manage the Territory, Protect the Environment, Evaluate the Cultural Heritage.* Copenhagen, Denmark: International Federation of Surveyors (FIG).

Dinn, D. F., B. D. Loncarevic, and G. Costello. 1995. "The effect of sound velocity errors on multi-beam sonar depth accuracy." In *Proc., Challenges of Our Changing Global Environment*, 1001–1010. New York: IEEE. https://doi.org/10.1109/OCEANS.1995.528559.

Eleftherakis, D., A. Amiri-Simkooei, M. Snellen, and D. G. Simons. 2012. "Improving riverbed sediment classification using backscatter and depth

residual features of multi-beam echo-sounder systems." *J. Acoust. Soc. Am.* 131 (5): 3710–3725. https://doi.org/10.1121/1.3699206.

Eleftherakis, D., M. Snellen, A. Amiri-Simkooei, D. G. Simons, and K. Siemes. 2014. "Observations regarding coarse sediment classification based on multi-beam echo-sounder's backscatter strength and depth residuals in Dutch rivers." *J. Acoust. Soc. Am.* 135 (6): 3305–3315. https://doi.org/10.1121/1.4875236.

Godin, A. 1998. "The calibration of shallow water multibeam echo-sounding systems." M.S. thesis, Dept. of Geodesy and Geomatics Engineering, Univ. of New Brunswick. http://www2.unb.ca/gge/Pubs/TR190.pdf.

Hare, R. 1995. "Depth and position error budgets for multibeam echo-sounding." *Int. Hydrogr. Rev.* 72 (2): 37–69.

Hare, R. 2001. "Error budget analysis for US naval oceanographic office (NAVOCEANO) hydrographic survey systems." Hattiesburg, MS: Hydrographic Science Research Center.

Hughes Clarke, J. E. 2003. "Dynamic motion residuals in swath sonar data: Ironing out the creases." *Int. Hydrogr. Rev.* 4 (1): 6–23.

Kannan, R., G. Latha, and M. P. Devi. 2015. "Optimum statistical gridding technique for multi beam echo sounder (MBES) data processing." In *Proc., Int. Symp. on Ocean Electronics (SYMPOL).* New York: IEEE. https://doi.org/10.1109/SYMPOL.2015.7581162.

Kongsberg. 2006. "EM 3002 multibeam echo sounder: The new generation high performance shallow water multibeam." Accessed August 20, 2018. http://www.bkmarine.no/index_htm_files/EM%203002%20Product%20description.pdf.

Lucieer, V., Z. Huang, and J. Siwabessy. 2016. "Analyzing uncertainty in multibeam bathymetric data and the impact on derived seafloor attributes." *Mar. Geod.* 39 (1): 32–52. https://doi.org/10.1080/01490419.2015.1121173.

Maleika, W. 2013. "The influence of track configuration and multibeam echosounder parameters on the accuracy of seabed DTMs obtained in shallow water." *Earth Sci. Inform.* 6 (2): 47–69. https://doi.org/10.1007/s12145-013-0111-9.

Maleika, W. 2015. "The influence of the grid resolution on the accuracy of the digital terrain model used in seabed modeling." *Mar. Geophys. Res.* 36 (1): 35–44. https://doi.org/10.1007/s11001-014-9236-6.

Maleika, W., M. Koziarski, and P. Forczmański. 2018. "A multiresolution grid structure applied to seafloor shape modeling." *ISPRS Int. J. Geo-Inf.* 7 (3): 119–133. https://doi.org/10.3390/ijgi7030119.

Maronna, R. A., R. D. Martin, and V. J. Yohai. 2006. *Robust statistics: Theory and methods.* Chichester, UK: Wiley.

Mohammadloo, T. H., M. Snellen, D. G. Simons, B. Dierikx, and S. Bicknese. 2018. "Minimum depth, mean depth or something in between?" *Int. Hydrogr. Rev.* 19: 45–53.

NOAA (National Oceanic and Atmospheric Administration). 2017. "Hydrographic survey specifications and deliverables." Washington, DC: NOAA.

Norbit. 2010. "Wideband multibeam sonar for high resolution bathymetry." Accessed August 20, 2018. https://norbit.com/media/PS-120005-21_WBMS-bathy_Pn_12003-AACDB4_A4.pdf.

Penney, D. 2018. "Qimera cube options dialogs." Accessed August 16, 2018. https://confluence.qps.nl/display/QM170/Qimera+CUBE+Dialogs.

Press, W. H., S. A. Teukolsky, W. T. Vettering, and B. P. Flannery. 1992. *Numerical recipes in C: The art of scientific computing.* 2nd ed. Cambridge, UK: Cambridge Univ.

Preston, J., A. Christney, S. Bloomer, and I. Beaudet. 2001. "Seabed classification of multibeam sonar images. In *Proc., MTS/IEEE Oceans 2001. An Ocean Odyssey*, 2616–2623. New York: IEEE. https://doi.org/10.1109/OCEANS.2001.968411.

QINSy. 2018. "How-to height—Tide and RTK." Accessed August 17, 2018. https://confluence.qps.nl/qinsy/en/how-to-height-tide-and-rtk-35587269.html.

Rousseeuw, P. J., and M. Hubert. 2011. "Robust statistics for outlier detection." *WIREs Data Min. Knowl. Discovery* 1 (1): 73–79. https://doi.org/10.1002/widm.2.

Snellen, M., K. Siemes, and D. G. Simons. 2009. "A model-based method for reducing the sound speed induced errors in multi-beam echo-sounder bathymetric measurements." In *Proc., OCEANS 2009-EUROPE.*, 1155–1162. New York: IEEE. https://doi.org/10.1109/OCEANSE.2009.5278103.

Teunissen, P. J. G., D. G. Simons, and C. C. J. M. Tiberius. 2006. *Probability and observation theory: An introduction.* Delft, Netherlands: Delft Univ. of Technology.

Valeport. 2018. "MiniSVP sound velocity profiler." Accessed August 18, 2018. https://www.valeport.co.uk/Products/Sound-Velocity/Sound-Velocity-Details/ProductID/4.

Vásquez, M. E. 2007. "Tuning the CARIS implementation of CUBE for Patagonian waters." M.S. thesis, Dept. of Geodesy and Geomatics Engineering, Univ. of New Brunswick. http://www2.unb.ca/gge/Pubs/TR251.pdf.

Zangeneh-Nejad, F., A. R. Amiri-Simkooei, M. A. Sharifi, and J. Asgari. 2017. "Cycle slip detection and repair of undifferenced single-frequency GPS carrier phase observations." *GPS Solut.* 21 (4): 1593–1603. https://doi.org/10.1007/s10291-017-0633-6.